Journal of Constructional Steel Research 166 (2020) 105905

Contents lists available at ScienceDirect

Journal of Constructional Steel Research

Improving the seismic performance of diagrid structures using buckling restrained braces

Saman Sadeghi, Fayaz R. Rofooei *

Civil Engineering Department, Sharif University of Technology, Tehran, PO Box 11155-4313, Iran

ARTICLE INFO

Article history:
Received 20 July 2019
Received in revised form 29 November 2019
Accepted 9 December 2019
Available online xxxx

Keywords:
Diagrid structures
Buckling restrained braces
Seismic performance factors
Incremental dynamic analysis (IDA)
Pushover analysis
Collapse margin ratio

ABSTRACT

The seismic performance of diagrids equipped with buckling restrained braces (BRBs) is investigated. In that regard, the effects of BRBs on the seismic performance characteristics of diagrids such as response modification factor, R, overstrength factor, Ω_0, ductility ratio, μ, and median collapse capacity, $\hat{S}_{CT}$, are evaluated. To this end, 6 three dimensional diagrid structures with various heights and diagonal angles are modeled using OpenSees program and are equipped with BRBs in a novel arrangement. Utilizing nonlinear static analysis, the seismic performance factors of models are evaluated. Subsequently, the median collapse capacity ($\hat{S}_{CT}$) of the models are determined by performing nonlinear dynamic analyses. The results indicate that using BRBs improve the seismic performance of the considered models due to accumulation of plastic damages in BRBs and a better distribution of plastic hinges over those models. The nonlinear static analyses indicate that for the original diagrid models, the response modification factor, R, ranges from 1.7–2.5, while the ductility ratio, μ, varies between 1.2 and 2.5, depending on the diagonal angles. Also, the results show that the Ω_0 remains fairly constant. However, in BRB equipped diagrids, the range of *R* increases to 2.4–3.3, while the ductility ratio μ varies in the range 2.1–3.1. Similar to regular diagrids, Ω_0 remains constant for BRB equipped models. Furthermore, the output of the dynamic analyses indicates that the $\hat{S}_{CT}$, which is a function of diagonal angles and generally increases by growing the diagonal angles, could rise up to 60% for diagrids equipped with BRB.

1. Introduction

After a long period of ignoring aesthetic aspects of brace elements in building constructions, now, the engineering societies are convinced to benefit from the appearance of these components as a symbol of concinnity in urban construction. One of the manifest examples of this trend is the diagrid system which has emerged as an innovative and adoptable approach to create not only the building structures but also constructions with various functionalities.

Over time people learnt how to increase the resistance of the building structures against lateral forces such as wind, soil pressure, water pressure, and earthquakes, by "use of oblique elements" [1]. Nonetheless, utilizing only pure triangulate modules to build a structure commenced in 20th century by Vladimir Shukhov in designing a radio tower (opened 1922). After that, triangulation concept assisted Walther Bauersfeld to construct the first geodesic dome, for a planetarium (opened 1926). Some years later, in 1953, Goldsmith [2], who majored civil engineering at the Illinois Institute of Technology, probably was the first person that academically investigated the diagrids. He proposed three different diagrid shapes that did not receive much attention, until one of them was utilized by Fazlur Khan [1] in designing the John Hancock Center in Chicago. In 1963, IBM building in Pittsburgh was constructed which can be considered as the most prominent example of shifting to diagrid structures. Fig. 1 shows some important diagrid structures built around the world [1].

Diagrids are more difficult to construct than other common tall buildings; the joints of diagrids are more complicated since up to six members may interconnect at each joint [3]. However, there are some reasons that may elucidate this new willingness of engineering community to use diagrids. The first reason is that the diagrid concept is a satisfying tool for the architects to create whatever they want [4]. Using this new solution to create elegant tall buildings with unusual shapes is undoubtedly due to the advantages of triangulation pattern of diagrids [1]. Triangulate tessellation of diagrids indeed makes them to enfold the building structures with any type of curved shape [5]. The second reason is that not only the diagrids are aesthetically satisfying, but they are also structurally efficient [6]. A diagrid structure inherently needs less material than other systems used to support the tall buildings [1], while it has a superior flexibility in plan since it is capable of not having interior and corner columns [7]. Diagrids respond to the gravity and lateral loads by axial reaction of their members rather than bending actions that is dominant in systems with vertical columns [8]. It makes

* Corresponding author.
E-mail addresses: Sadeghi_Saman@mehr.sharif.ir (S. Sadeghi), rofooei@sharif.edu (F.R. Rofooei).

https://doi.org/10.1016/j.jcsr.2019.105905
0143-974X/

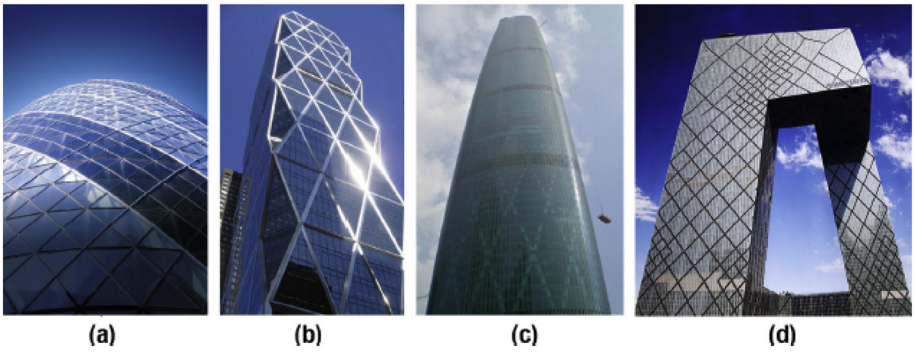

Fig. 1. (a) Swiss Re Tower, (b) Hearst Tower, (c) Guangzhou West Tower, (d) China Central Television (CCTV) Headquarters [1].

them to be a comparatively stiff system that easily passes the displacement requirements of tall buildings while using less material.

As an example, utilizing diagrid system for Hearst Tower led to using 20% less material than adopting a moment resisting frame system [9]. Although in some tower buildings such as Lotte Super Tower, the interior core provides additional strength against lateral loads [10], diagrids basically are core dispensable, and this can be considered as one of the prominent factors which promotes the efficiency of diagrids. On the other hand, the axial action of the diagonal elements located on the perimeter of diagrids provides high shear rigidity for this structural system [11]. Even the buildings with braced inner cores have much less stiffness than the diagrids despite the fact that the diagrid diagonals can be designed just for the gravity loads [11]. The effects of shear lag which increases stress in perimeter columns and reduces structural efficiency [7], are much less in diagrids with regard to other tubular systems due to their higher shear stiffness.

Despite of all aforementioned privileges of diagrids, limited research, which mainly focuses on the elastic characteristics of this structural system, has been carried out to investigate the performance of diagrids. For example, [1,5,11,12] propose methods to elastically pre-design the diagrids under wind load. The reluctance of scholars to numerically and/or experimentally assess the seismic performance of diagrids is expectable, as most of the constructed diagrids are located in low seismic regions.

Diagrids generally show brittle behavior under seismic loads. Baker et al. [13] conducted nonlinear static and dynamic analyses on a single 8-story diagrid model to evaluate its seismic performance factors (SPFs). They adopted the FEMA P695 [14] criteria and determined the response modification factor (R-factor) and the overstrength factor (Ω_0) of the model to be 3.64 and 1.5, respectively. Kim et al. [15] confirmed that the diagrids exhibit a brittle behavior and showed that the collapse of diagrids can occur in drift ratios less than 1%. In an approach which was not economically practical, they replaced all diagonal members of diagrids with BRBs. That led to the formation of plastic hinges more widely and increased the structural ductility. Also, a new configuration was proposed for diagrid structures with shear-link fuse that enhanced their ductility and reduced the residual displacements [16]. While there is no experiment on performance of a diaigrid structure under earthquakes, some experiments [17–19] have investigated the performance of the diagrid joints (the intersection of the diagonal elements) under cyclic and static loads. Furthermore, application of concrete filled steel tubes (CFST) in diagrids, the optimum angle of the diagonals, and the progressive collapse of diagrids, have been studied by researchers [20–22].

This paper investigates the seismic performance of diagrids equipped with BRBs. Research indicates that BRBs can be an effective tool to control damage and dissipate seismic energy [23,24]. In that regard a number of 6 three dimensionally diagrid models with 8 and 12 stories and three different diagonal angles of 45°, 63.4°, and 71.5° are modeled using the open source finite element framework, OpenSees software [25]. This range of structural height has been selected for two reasons: first, the number of mid- and low-rise diagrids is increasing throughout the world, and second, to opt the height range that is more sensitive and susceptible to seismic excitations in comparison to the wind loads. All models are prepared using the regular diagonal elements with buckling capability. In the next step the same models are constructed by employing the BRB elements as some of their diagonals. Conducting extensive nonlinear dynamic and static analyses, the SPFs of all the models with and without BRBs are determined.

2. Designing and modeling diagrid archetype models

As already mentioned, the diagrids can be constructed in a variety of shapes. However, this paper considers the diagrids with ordinary configurations in order to investigate the effects of some main parameters such as the diagonal angles, structural height, and the behavior of diagonal elements on their seismic response. Consequently, a number of 6 diagrid archetype models with 8 and 12 number of stories are considered. The models have the same square plan with four bays along the orthogonal directions each 9 m wide, so the footprint of all models is 36 m × 36 m, with a story height of 4.5 m as shown in Fig. 2. Also, as presented in Fig. 3, three angles of 45°, 63.4° and 71.5° are chosen for the diagonals. As already mentioned, all the diagrid frames are located on

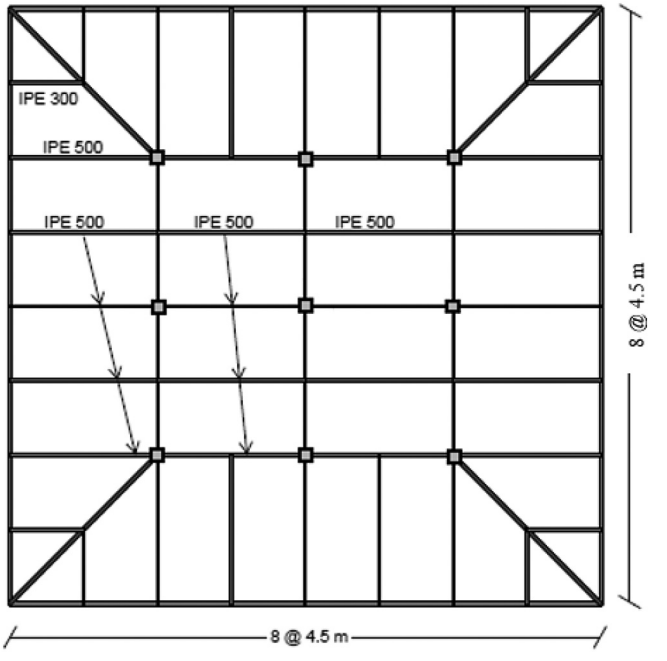

Fig. 2. Floor framing plan of the models.

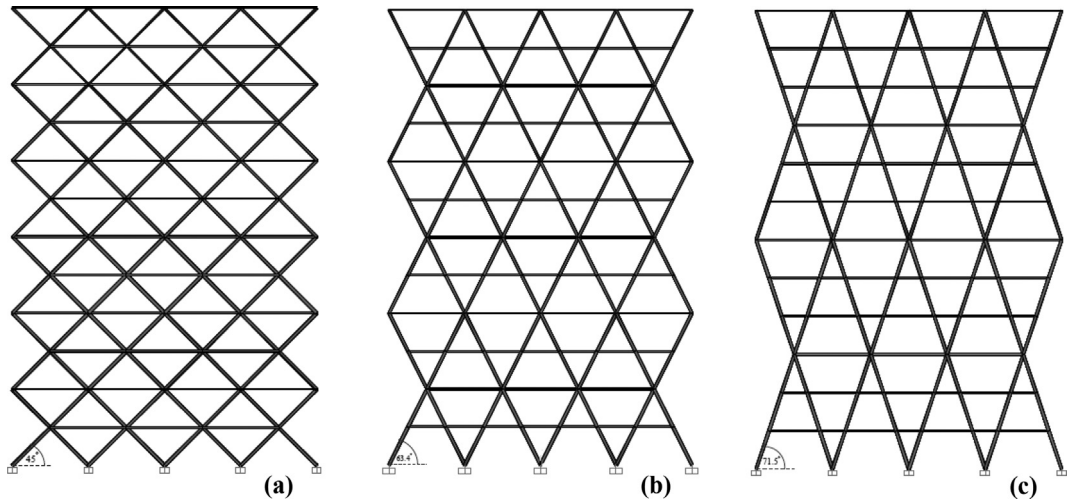

Fig. 3. Facade of 12-story diagrid models: (a) 12-story-45°, (b) 12-story-63.4°, (c) 12-story-71.5°.

Table 1
Design response spectrum parameters.

S_S	S_1	F_a	F_v	S_{MS}	S_{M1}	S_{DS}	S_{D1}
1.5	0.6	1	1.5	1.5	0.9	1	0.6

the perimeters of the models. Also, 9 columns are placed in the middle space of the models for transferring the gravity loads. These columns are connected to the perimeter diagrid frames by pin-ended beams to prevent them from contributing to the lateral load carrying capacity of the diagrid system.

All the models are designed according to the ASCE/SEI 7-10 [26], with a R-factor of 3.6 as proposed by Baker et al. [13], assuming all the diagrids are located on soil type D and Seismic Design Category (SDC) D. The displacement amplification factor (C_d) is supposed to be equal to R-factor as suggested by FEMA P695 [14]. Also, the over-strength factor (Ω_0) was not used in design process, as it is not clear which critical members of diagrids should be designed considering the Ω_0. Besides, office functionality is considered for the occupancy of these structural models with the related risk category and seismic importance factors of II and 1, respectively. Since the diagrid systems are not yet recognized as one of the standard lateral load carrying systems by seismic design codes, the special concentric braced frames requirements are utilized as the complementary criteria to design the diagrids. Equivalent static and response spectrum analysis methods are employed to design the models with the design spectrum parameters represented in Table 1, assuming that the structures are located in a high seismic region. The gravity dead and live loads are assumed as 650 kg/m^2 and 400 kg/m^2, respectively. Tubular sections are used for all diagonals, perimeter beams and the central gravity columns with the gravity middle beams selected as I-shaped sections. The steel material used for all members is of Grade 50 with yield stress equal to 344.7 MPa. Table 2 shows the designed diagonal sections of the selected models.

As discussed before, the diagrid structures gain their stability and rigidity through three dimensional tessellation of triangles. Basically, components of triangle modules counter the shear and flexural demands by axial reactions regardless of their connection type; as a result, the performance of diagrid system is highly reliant on the model that describes axial behavior of its elements. Using the capability of fiber section modeling and the implemented co-rotational transformation in the OpenSees software, buckling and post buckling behavior of an axial member can be simulated appropriately by a physical-theory-based element proposed by Uriz [27]. The axial member is divided into at least two equal parts which are connected to each other by applying a small imperfection at the connection point. Nonlinear hysteretic material is assigned to each fiber of the section, and a proper amount of imperfection is allocated to the middle of the element. When these properties are combined with the co-rotational theory, large deformations of the element are captured, and buckling can be simulated.

The previous research [28] indicates that the values of out of straightness imperfection are generally in the range of $0.001L$ — $0.005L$, where L is the total length of the element. In this study, to properly simulate the buckling load of the axial members, an imperfection of $0.005L$ is assumed for the diagonal elements. The section of this force-based nonlinear beam-column element is divided into 3 fibers along the thickness and 5 fibers along the edges. Uniaxial Menegotto-Pinto steel material (Steel02) is assigned to each fiber of the section. Other parameters of the Steel2 material in the OpenSees program are defined as the yield stress $F_y = 344.7$ *MPa*, the Young's modulus $E = 199.9$ *Gpa*, strain hardening ratio $b = 0.003$, the default values of $R_0 = 18.5$, $cR_1 = 0.925$, $cR_2 = 0.15$, to control the transition from elastic to plastic branch, and the parameters $a_1 = 0.0005$, $a_2 = 0.01$, $a_3 = 0.0005$, $a_4 = 0.01$, that are employed to account for the cyclic isotropic hardening [27]. Moreover, the Gauss-Lobatto numerical integration with 5 integration points along the element is considered for the analysis. This nonlinear beam-column element simulates the buckling and overall post buckling behavior of an axial member. To simulate fracture of the

Table 2
Designed diagonal sections for diagrid models.

8-story-45°	Story	8-story-63.4°	Story	8-story-71.5°	Story	12-story-45°	Story	12-story- 63.4°	Story	12-story-71.5°	Story
Tube 300 × 300 × 22.2	1,2	Tube 280 × 280 × 20	1,2	Tube 280 × 280 × 20	1,2,3	Tube 320 × 320 × 28	1,2	Tube 320 × 320 × 22.2	1,2	Tube 320 × 320 × 22.2	1,2,3
Tube 260 × 260 × 22.2	3,4	Tube 260 × 260 × 22.2	3,4	Tube 260 × 260 × 20	4,5,6	Tube 300 × 300 × 25	3,4	Tube 300 × 300 × 22.2	3,4	Tube 320 × 320 × 20	4,5,6
Tube 220 × 220 × 22.2	5,6	Tube 260 × 260 × 17.5	5,6	Tube 260 × 260 × 16	7,8	Tube 300 × 300 × 20	5,6	Tube 280 × 280 × 20	5,6	Tube 260 × 260 × 20	7,8,9
Tube 200 × 200 × 16	7,8	Tube 220 × 220 × 16	7,8			Tube 260 × 260 × 20	7,8	Tube 260 × 260 × 20	7,8	Tube 260 × 260 × 16	10,11,12
						Tube 220 × 220 × 20	9,10	Tube 240 × 240 × 16	9,10		
						Tube 200 × 200 × 16	11,12	Tube 220 × 220 × 16	11,12		

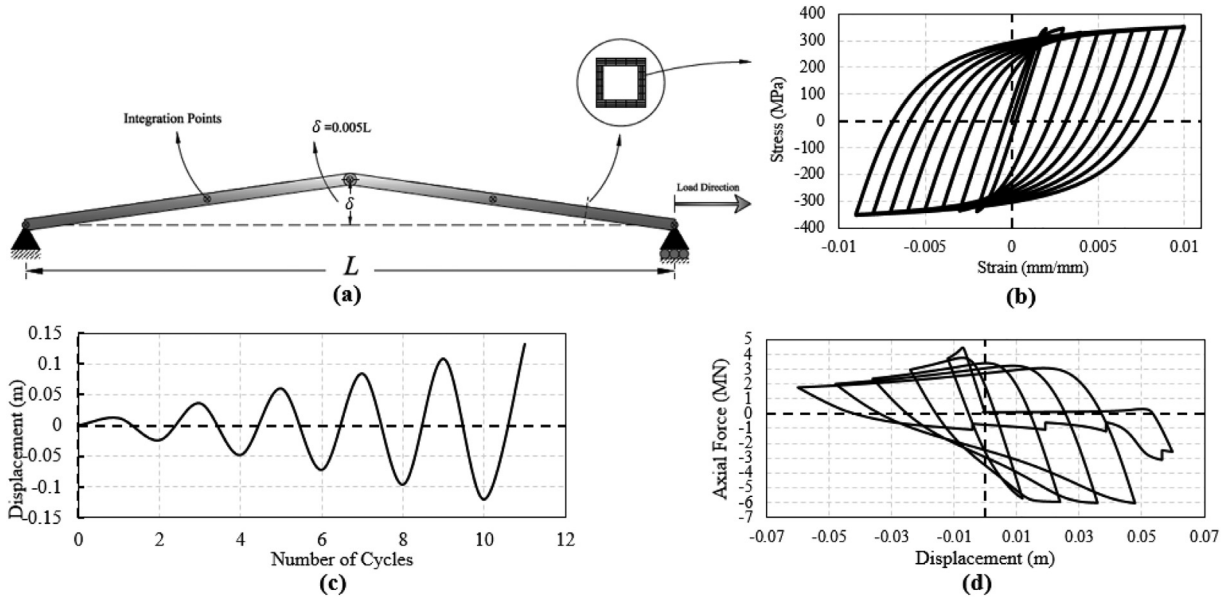

Fig. 4. The nonlinear beam-column element: (a) initial imperfection, (b) behavior of the material of the fibers, (c) cyclic load history and (d) force-displacement behavior of the element.

element under monotonic and cyclic loading, properties of fatigue material are attached to the uniaxial Steel02 material. Fatigue material is available in OpenSees program (uniaxialMaterial fatigue) which its two main parameters are taken as $m = -0.5$ and $\varepsilon_0 = 0.095$, according to Uriz's recommendation. Although the aforementioned element modeling do not consider the local buckling, but the parameters of fatigue material have been calibrated in a way to account for effects of local buckling. Fig. 4 represents the behavior of this nonlinear axial element. The validity of this model has been verified based on the results of numerous experimental tests conducted by Uriz and other researchers [27].

As mentioned before, in order to leave the entire lateral load bearing role to the perimeter diagrid frames, the central boxed-section gravity columns are connected to the perimeter diagrid frames by pin-ended beams. These gravity beams that are assigned I-shaped sections, transfer a portion of the gravity loads to the diagrid perimeter nodes. These members are modeled as pin-ended elements (truss element), while the central columns are modeled as elastic members (elastic BeamColumn element) to prevent them from having plastic behavior due to large displacements. The P-Delta coordinate transformation command is employed to include the P-Delta second-order effects in modeling the gravity columns. The floor system was not modeled, but to simulate the effects of rigid floor, all nodes of each level were constrained using the command "rigidDiaphragm".

On the other hand, a common-numerical approach of modeling the BRBs is to model them as a one-dimensional truss element. Fig. 5 shows the general configuration of a BRB element. The length of the three main segments of BRB are defined as: the core segment length (L_c), the transitional segment length (L_t), and the connection segment length (L_j). Some studies [27,29] indicate that L_c can be taken as 70% of total length of BRB (L_w). Moreover, the L_t and L_j are selected as 6% and 24% of the L_w, respectively. The cross section of the transitional segment (A_t) and connection segment (A_j) are selected such that $A_t/A_c = 2.0$ and $A_j/A_c = 3.0$, respectively, where A_c is the cross section area of the core segment [29].

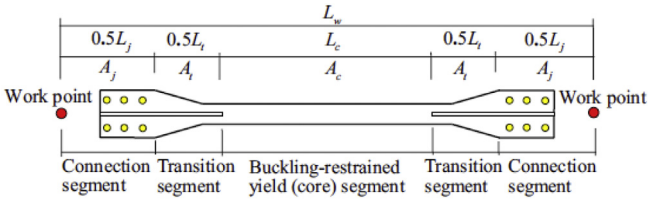

Fig. 5. General configuration of a BRB member [29].

The BRB is modeled as a truss element by defining its cross sectional area and material type. Material of BRB is defined as a one dimensional nonlinear steel material referred to as "SteelBRB", based on elasto-plastic model developed by Zona and Dall'Asta [31]. This rheological model have well been calibrated against experimental tests done by different researchers [30,32–34]. Employing the test results of Merrit et al. [30], as shown in Fig. 6, the parameters of the command "SteelBRB" are considered as:

The modulus of elasticity, $E = 199.9\ GPa$,

The initial yield force, $\sigma_{y0} = 248.2\ MPa$,

The maximum tension yield force of fully saturated isotropic hardening condition, $\sigma_{yT} = 414.49\ MPa$,

The constant of the plastic flow in tension, $\alpha_T = 0.6$,

The ratio of post yield stiffness (K_1^+) to initial stiffness (K_0^+) in tension, $\beta_T = 0.1$,

The hardening constant in tension, $\delta_T = 0.2$,

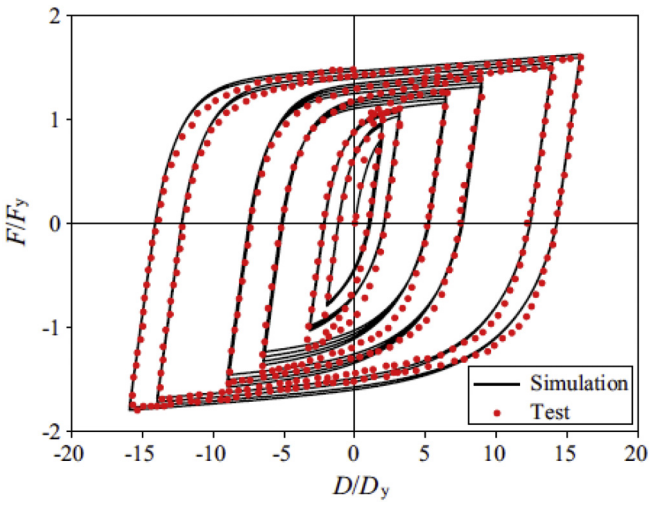

Fig. 6. Comparison of the results obtained from tests by Merrit [30] and the model prediction [31].

The maximum compression yield force of fully saturated isotropic hardening condition, $\sigma_{yC} = 464.23\ MPa$,

The constant of the plastic flow in compression, $\alpha_C = 0.4$,

The ratio of post yield stiffness (K_1^-) to initial stiffness (K_0^-) in compression, $\beta_C = 0.01$,

The hardening constant in compression, $\delta_T = 0.15$,

The connection and the transitional segments of BRB are not modeled and just one pin-ended truss element with the length L_w is placed between two nodes of the story. Thus, to achieve the actual behavior of BRB, the elastic stiffness of the truss element is adjusted by the following equation [29]:

$$E_{eff} = K_{eff}\frac{L_w}{A_c} = \frac{E_b A_c A_t A_j}{L_c A_t A_j + L_t A_c A_j + L_j A_c A_t}\frac{L_w}{A_c} = E_b\left(\frac{A_t A_j L_w}{L_c A_t A_j + L_t A_c A_j + L_j A_c A_t}\right) \quad (1)$$

where E_{eff} and K_{eff} are the effective modulus of elasticity and effective axial stiffness of the modeled BRB, respectively. The E_b is the modulus of elasticity of the BRB material which is considered as *199.9 GPa*. It is also assumed here that all plastic deformation of a BRB is accumulated in the core segment, while Uriz indicates that axial deformations of gusset plates of the connection segments are in the order of 10–15% of the total brace elongation. However, the accuracy of using a truss element to simulate the behavior of BRBs is satisfactory and effects of flexural components in global behavior of BRBs can be neglected [27]. For dynamic analyses, Rayleigh damping is employed by assigning 2% damping ratio for the first and fifth modes of the models.

3. Equipping the diagrid structural models with BRBs

Two approaches could be considered to equip the archetype diagrid models with BRBs. In the first approach, all the diagrid diagonals could be replaced with BRBs which would obviously be very costly. Alternatively, only the diagonals with larger demands (caused by lateral loading) in each story could be considered for replacement by BRBs. Fig. 7 shows the distribution of relative axial forces of the diagonal members that are obtained according to the equivalent lateral load analysis of ASCE 7-10 [26] for different diagonal angles. As this figure illustrates, the axial forces of the diagonals are normalized with respect to the maximum axial force. Due to the symmetric configuration of the models, just normalized forces of the left half of the models are shown in Fig. 7. As the results indicate, in each bay, the axial force of the diagonal members are not equal, while in some cases they might be very close (some ratios have become equal in the upper stories just because of neglecting the third digit after decimal points). Hence, replacing the diagonals with greater axial forces by BRBs causes the plastic deformation to be mainly concentrated in the BRBs before minor occurrence of yielding or buckling in the other adjacent unchanged diagonal members. According to this criterion, only one-half of the diagonal members of the diagrids in each story need to be replaced by BRBs in a symmetric way. To further increase the efficiency of the BRB elements in dissipating the seismic energy input, the yield stress of the BRBs can be considered to be slightly less than the buckling stress of the other regular diagonals.

Therefore, in the considered models, half of the diagonals (4 elements) that have greater normalized forces are replaced by the BRBs in each story. In addition, since the buckling stress of the initial diagonal members of the diagrids were between 0.75 and 0.85 times the member's yield stress (F_y), the yield stress of BRBs members was assumed to be 248.2 *MPa*.

The dynamic characteristics of the diagrid models are presented in Table 3. As it is shown, the natural periods of the initial and BRB-equipped models are almost the same and the stiffness of the initial models do not change after being equipped by BRBs.

4. Nonlinear static analyses

To validate the prepared nonlinear models and to evaluate the ductility ratio (μ), the over-strength factor (Ω_0), the ductility reduction factor (R_μ) and the response modification factor (R) of the diagrid models, pushover analyses are conducted. Initially, the diagrid structures are statistically analyzed under the following gravity load combination:

$$1.05Q_D + 0.25Q_L \quad (2)$$

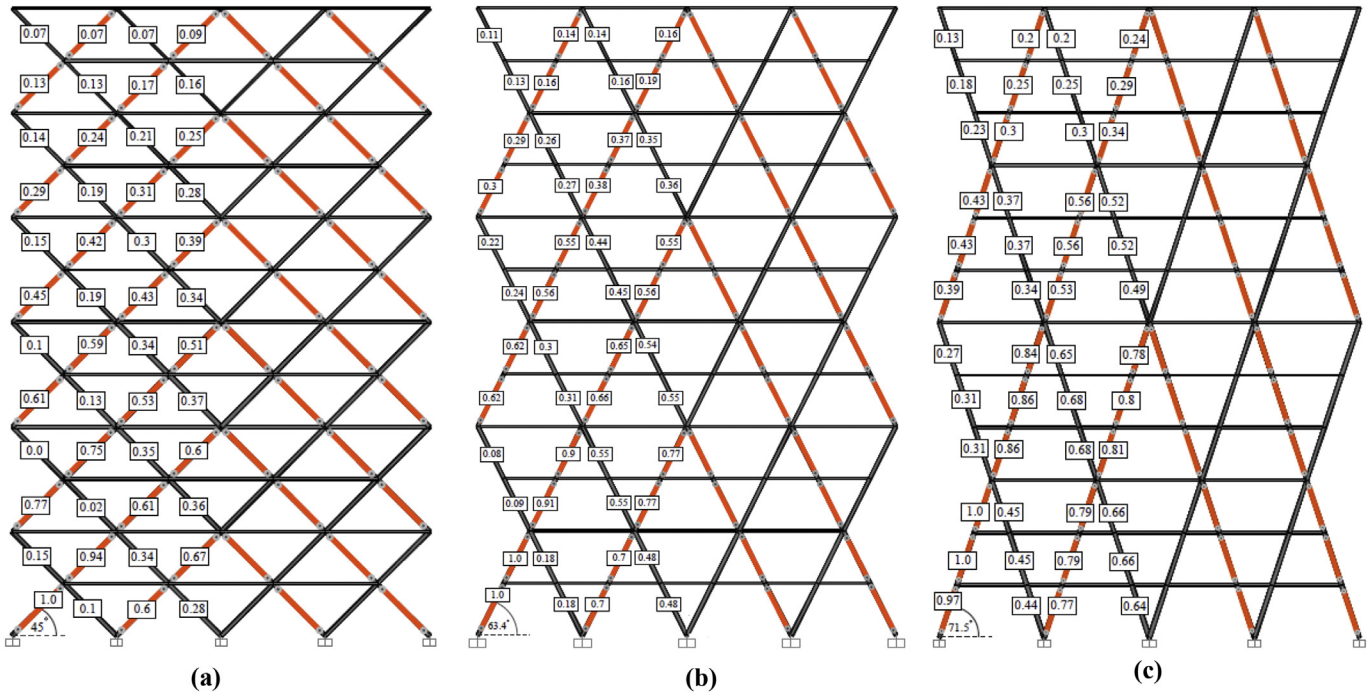

Fig. 7. The normalized axial forces of the diagonals under applied lateral loadings that need to be replaced by BRB members in 12-story diagrid models: (a) 45°, (b) 63.4°, and (c) 71.5°.

Table 3
The natural periods of the first three modes of vibration for the initial and BRB-equipped models [seconds].

	8-Story-45°		8-Story-63.4°		8-Story-71.5°		12-Story-45°		12-Story-63.4°		12-Story-71.5°	
	Initial	BRB-equipped	Initial	BRB-equipped	Initial	BRB-equipped	Initial	BRB-equipped	Initial	BRB-equipped	Initial	BRB-equipped
Mode 1	0.65	0.62	0.79	0.8	1.13	1.12	0.98	0.94	1.15	1.11	1.38	1.35
Mode 2	0.65	0.62	0.78	0.78	1.11	1.10	0.98	0.94	1.15	1.11	1.37	1.34
Mode 3	0.25	0.21	0.46	0.50	0.65	0.71	0.32	0.30	0.54	0.55	0.65	0.71

where Q_D and Q_L represent the dead and live loads, respectively. Then, using appropriate lateral load pattern, the diagrids are incrementally pushed up to the target displacement δ_t. The ASCE 41-13 [35] suggested load pattern is as follows:

$$F_x \propto m_x \varnothing_{1,x} \tag{3}$$

where F_x is the horizontal force acting at the level of x-story, m is the mass of the x-story, and $\varnothing_{1,x}$ is the amplitude of the fundamental mode at the level of x-story. Next, to evaluate the yield and ultimate strengths and deformations, the constructed pushover curves are linearized according to ASCE 41-13 [35] code.

Using the linearized pushover curves and the method proposed by Uang [36], the SPF of the diagrid models are evaluated. In this methodology, the response modification factor is determined by the following equation:

$$R = \frac{V_e}{V_s} = \frac{V_e}{V_y} \times \frac{V_y}{V_s} = R_\mu \times \Omega_0 \tag{4}$$

where V_e is maximum elastic base shear force, V_s is the base shear in which first significant yield occurs in the system and is approximated from the results of pushover analysis, V_y is the base shear corresponding to yield strength, and R_μ is the strength reduction factor. Also, V_e can be approximated by multiplying the design base shear (V) by the design R factor (which is equal to 3.6). Likewise, V_y is determined from pushover curve shown in Fig. 8.

The results of the pushover analyses of diagrid models shown in Fig. 9 indicate that the application of BRB significantly improves the softening part of the pushover curves. Table 4 presents the results for the SPFs extracted from the linearized pushover curves.

Besides, the important parameters of the conducted pushover analyses such as C_0 (the coefficient relating the roof displacements to the fundamental mode of the structure), T_e (the effective period), δ_t (target displacement), the yield displacement (δ_y), ultimate displacement (δ_u), and ductility ratio (μ) are presented in Table 5. Fig. 10 explains the variation of SPFs as a function of diagonal angles. This figure shows that the over-strength factor (Ω_0) is fairly constant for different diagonal angles with average values of 1.23 for 8-story models and 1.17 for 12-story models. As one could observe, both the R_μ and R increase with growing diagonal angles. This trend is better shown in the shorter (8-story) models. In 12-story models, both R_μ and R decrease for diagonal angles greater than 63.4°. The same pattern is also observed in the BRB equipped models. To better understand the effects of equipping the diagrid models by BRBs, a performance index (PI) is defined as the ratio of a seismic parameter of the BRB equipped model to the same parameter of the initial model as the following:

$$PI = \frac{SPF\ of\ BRB\ equipped\ model}{SPF\ of\ Initial\ model} \tag{5}$$

Fig. 11 shows the variation of PI for the Ω_0, R_μ, and R as a function of diagonal angles, which indicates that the PI for all considered SPFs is greater than one. So, employing the BRBs in the diagrid structures improves their seismic performance. But the level of improvement for 12-story models is generally greater than 8-story models. Mean value of PI of R-factor for 8-story and 12-story models are equal to 1.24 and 1.59, respectively. For 8-story models, by increasing the diagonal angles, the PI of R-factor reduces; thus, the BRBs are more efficient in improving the seismic performance of 8-story-45° diagrid models. For 12-story models, larger diagonal angles increases the PI of R_μ while PI of R-factor attains its maximum at angle of 63.4°. Therefore, the BRB has the best performance in improving the SPF of 12-story-63.4° diagrid system. In this model, using BRBs increases the R-factor from 1.97 to 3.28, indicating an increase of 66% for the R-factor of initial diagrid model.

Fig. 12 clearly demonstrates the effect of buckling of the diagonal members and yielding BRBs on the overall performance of the diagrid models. The shown pushover curves belong to the initial and BRB equipped 8-story-45° diagrid model. In the initial model, a sharp decrease can be seen in the pushover curve caused by the buckling of

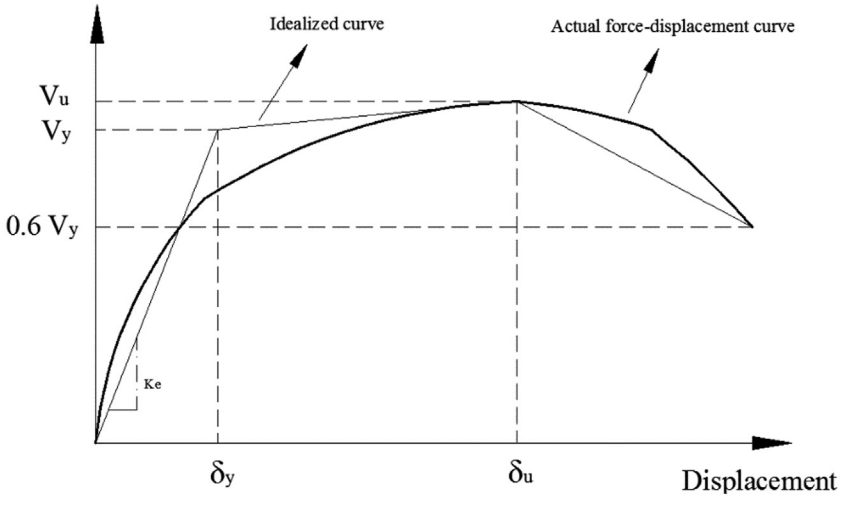

Fig. 8. Actual and idealized pushover curves.

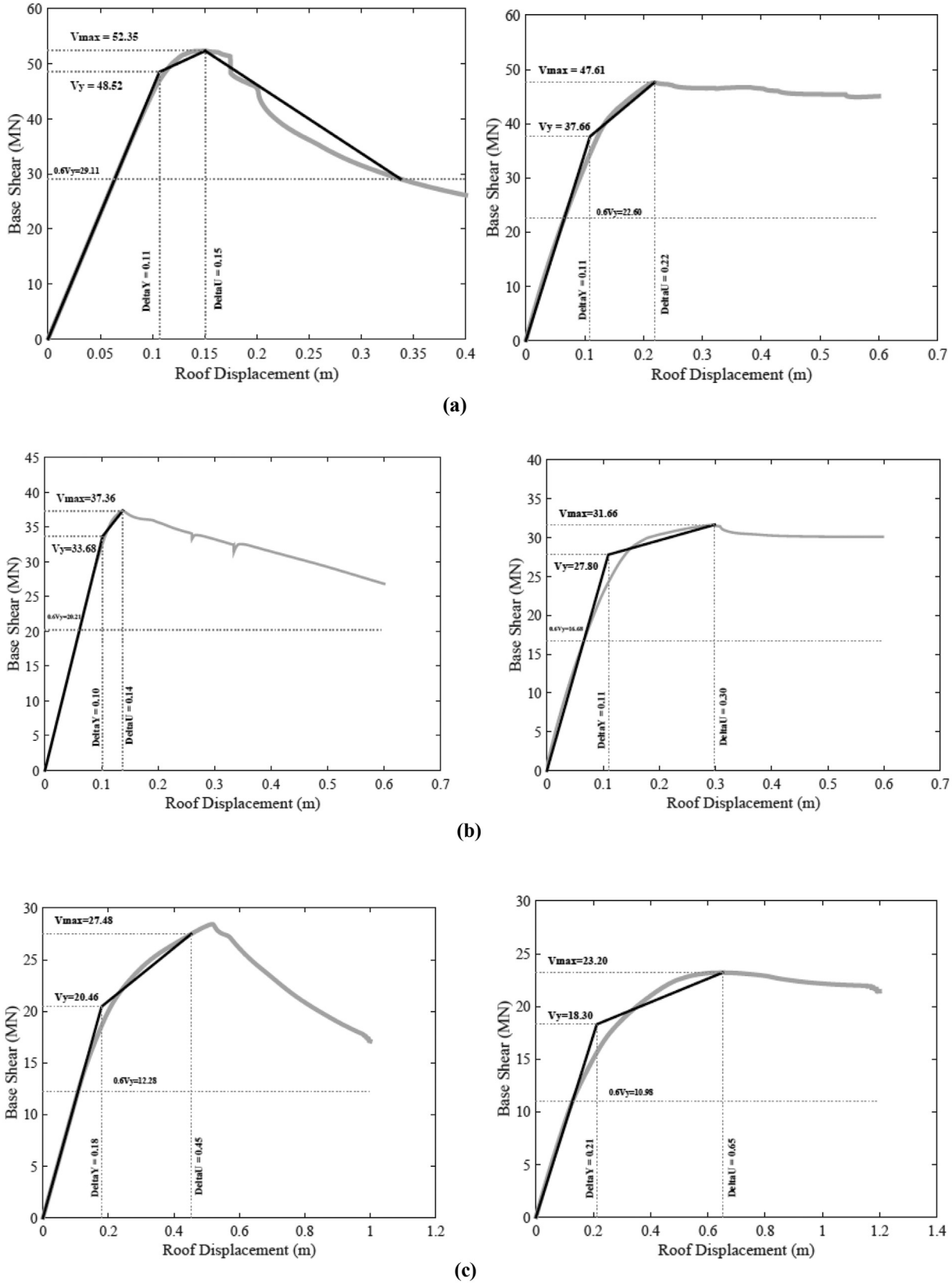

Fig. 9. The actual and linearized pushover curves (Left: The initial diagrid models, Right: The BRB equipped models): (a) 8-story-45°, (b) 12-story-45°, (c) 8-story-63.4°, (d) 12-story-63.4°, (e) 8-story-71.5°, (f) 12-story-71.5°.

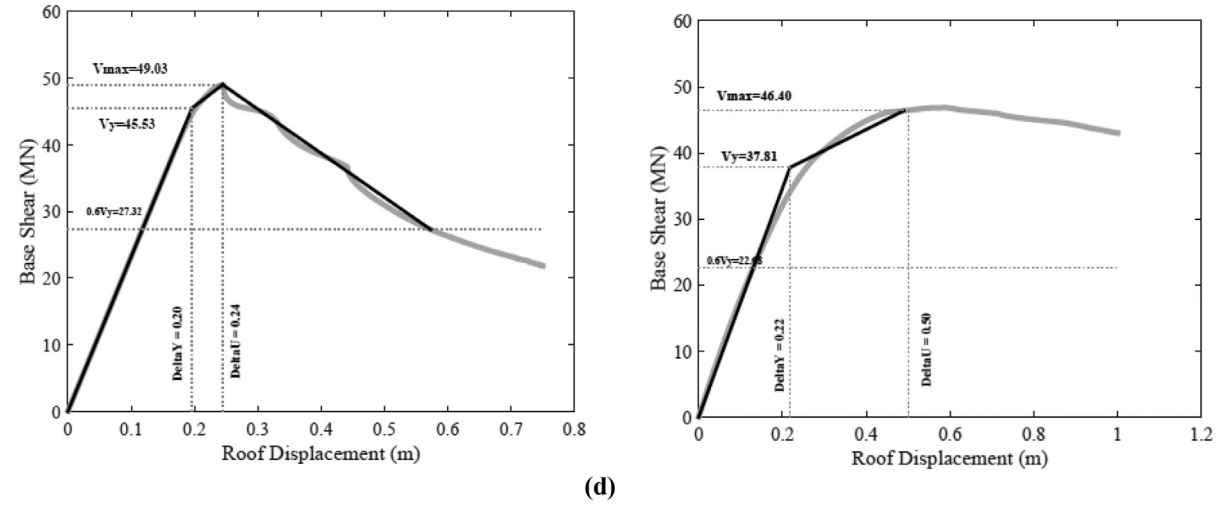

(d)

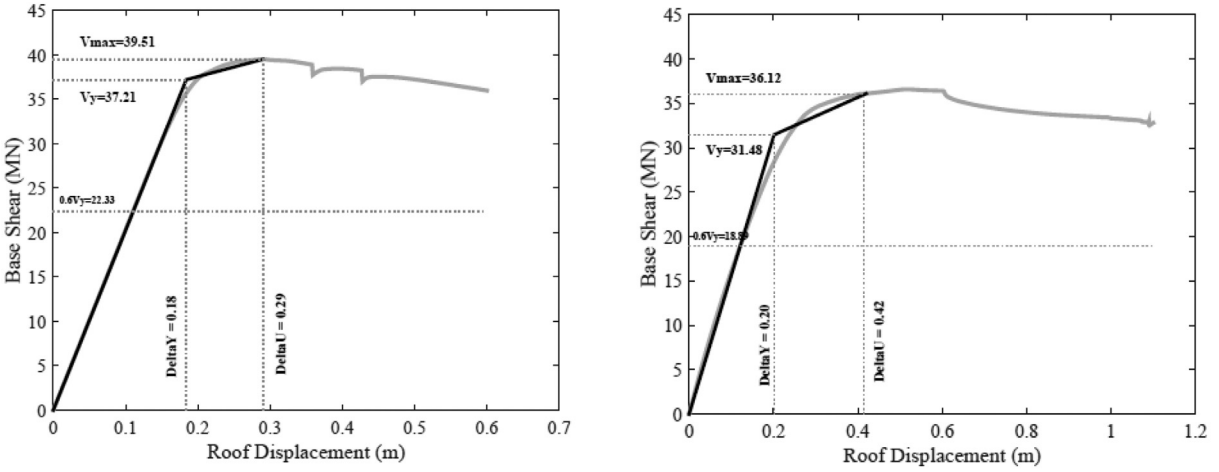

(e)

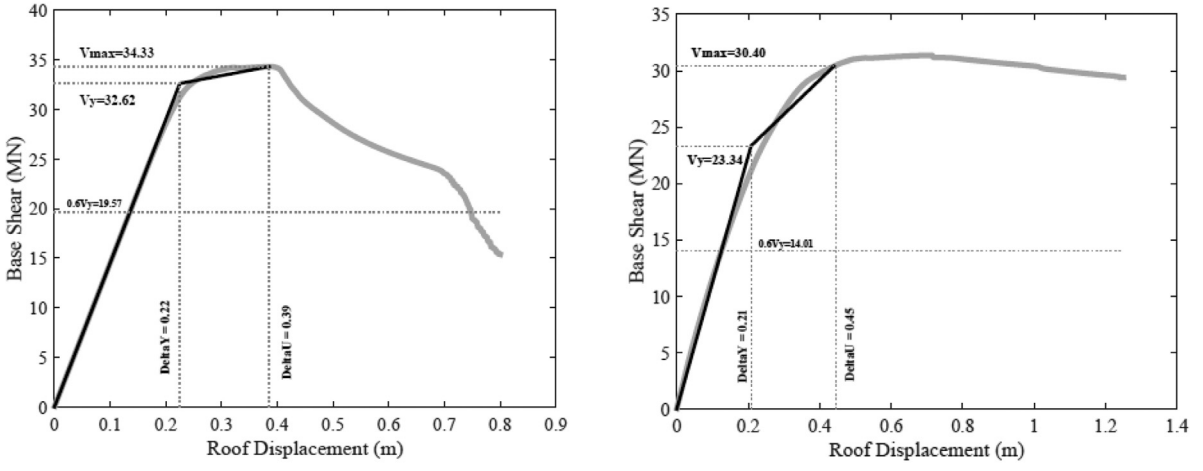

(f)

Fig. 9 (*continued*).

the diagonal members of the first 4 floors of the model. On the other hand, in the BRB equipped model, the yielding BRBs is the dominating mechanism of energy dissipation and it can be observed that the shape of the pushover curve is highly dependent on the behavior of BRBs. In fact, after yielding of the BRBs, the diagrid model experiences its maximum strength without any subsequent abrupt change in the base shear. In the BRB equipped model, just five of the un-retrofitted diagonal members buckle while most of the replaced diagonals with BRB

Table 4
The results of the pushover analyses.

Model	V_e (MN)	V_y (MN)	V_s (MN)	R_μ	Ω_0	R
8-St 45°	75.09	48.52	38.1	1.54	1.27	1.95
8-St 45° (BRB equipped)	75.09	37.66	28.0	2.0	1.34	2.68
8-St 63.4°	57.25	33.68	28.4	1.7	1.18	2.0
8-St 63.4° (BRB equipped)	47.61	27.6	20.0	1.72	1.38	2.37
8-St 71.5°	40.1	20.46	16.2	1.96	1.26	2.47
8-St 71.5° (BRB equipped)	40.36	18.3	13.8	2.2	1.32	2.9
12-St 45°	70.4	45.53	40.4	1.54	1.12	1.72
12-St 45 (BRB equipped)	75.1	37.81	28.5	1.98	1.32	2.61
12-St 63.4°	60.58	37.21	30.37	1.62	1.22	1.97
12-St 63.4 (BRB equipped))	62.82	31.48	19.2	2.0	1.64	3.28
12-St 71.5°	49.2	32.62	27.64	1.5	1.18	1.77
12-St 71.5° (BRB equipped)	50.67	23.34	17.78	2.17	1.31	2.84

Table 5
The different parameters obtained from the pushover analyses.

Model	C_0	T_e (s)	δ_y (m)	δ_u (m)	μ
8-St 45°	1.38	0.64	0.11	0.15	1.36
8-St 45° (BRB equipped)	1.41	0.6	0.11	0.22	2.0
8-St 63.4°	1.07	0.95	0.1	0.14	1.4
8-St 63.4° (BRB equipped)	1.13	1.07	0.11	0.3	2.72
8-St 71.5°	1.55	1.21	0.18	0.45	2.5
8-St 71.5° (BRB equipped)	1.56	1.21	0.21	0.65	3.1
12-St 45°	1.45	0.94	0.2	0.24	1.2
12-St 45 (BRB equipped)	1.45	0.96	0.22	0.5	2.27
12-St 63.4°	1.28	1.1	0.18	0.29	1.61
12-St 63.4° (BRB equipped)	1.26	1.25	0.2	0.42	2.1
12-St 71.5°	1.22	1.41	0.22	0.39	1.77
12-St 71.5° (BRB equipped)	1.17	1.5	0.21	0.45	2.14

elements yield, which in a way verifies the efficacy of the proposed application of the BRBs. Moreover, the distribution of the yielded and buckled members is more uniform in the BRB equipped model. The maximum strength of the retrofitted structure is slightly lower than the initial model because the yield stress of the BRB elements is assumed to be less than the buckling stress of the un-retrofitted diagonal elements.

5. Nonlinear dynamic analyses

5.1. Ground motion records

The far-field ground motion records provided by FEMA P695 are selected to investigate the collapse performance of the structures through performing nonlinear dynamic analyses [14]. The far-field record set includes 22 horizontal record pairs of strong ground motions from sites located at a distance greater than or equal to 10 km from the fault rupture line. The number of records is large enough to statistically evaluate collapse behavior of structures.

5.2. Evaluating the collapse margin ratio using incremental dynamic analyses

The collapse margin ratio (CMR) is defined as the ratio of the median collapse capacity ($\hat{S}_{CT}$) to the spectral intensities of the maximum considered earthquake (MCE) at the fundamental period of the structure (S_{MT}), as indicated by Eq. (6). The CMR is considered as the adjusted amount of the S_{MT} where 50% of the ground motions trigger collapse and represents the way the MCE ground

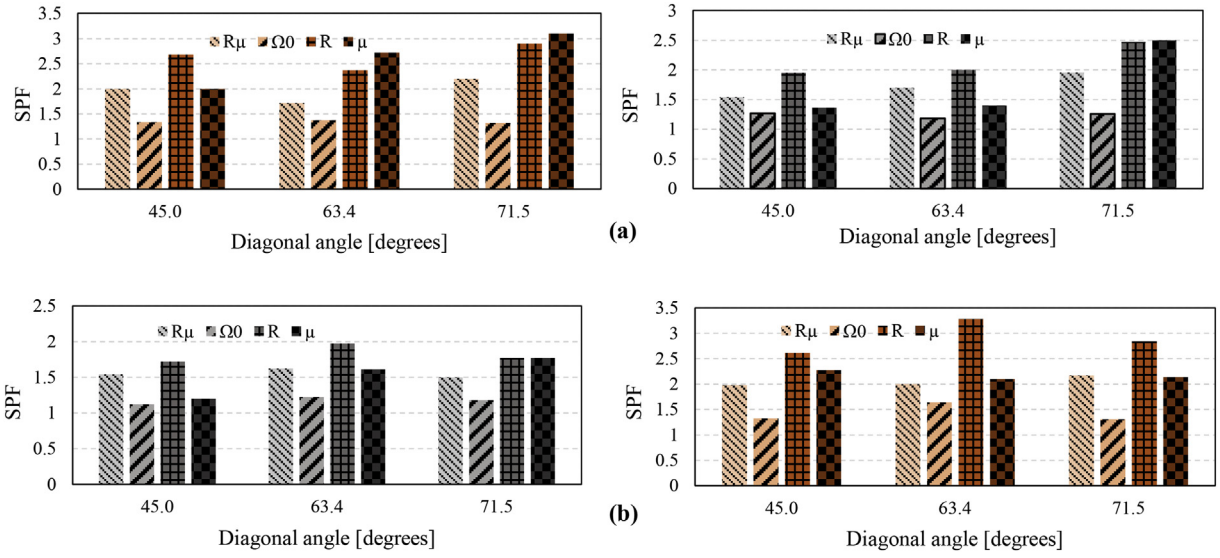

Fig. 10. Variation of SPFs of the diagrid models vs diagonal angles (left: Initial models, right: BRB equipped models): (a) 8-story models, (b) 12-story models.

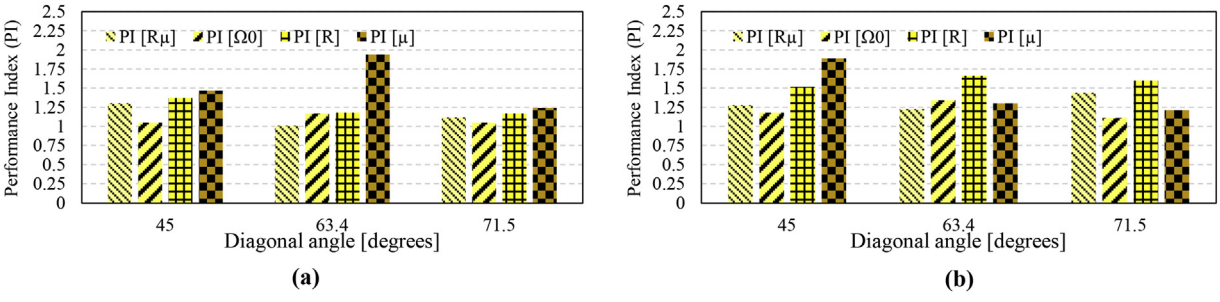

Fig. 11. Variation of PI vs diagonal angles: (a) 8-story models, (b) 12-story models.

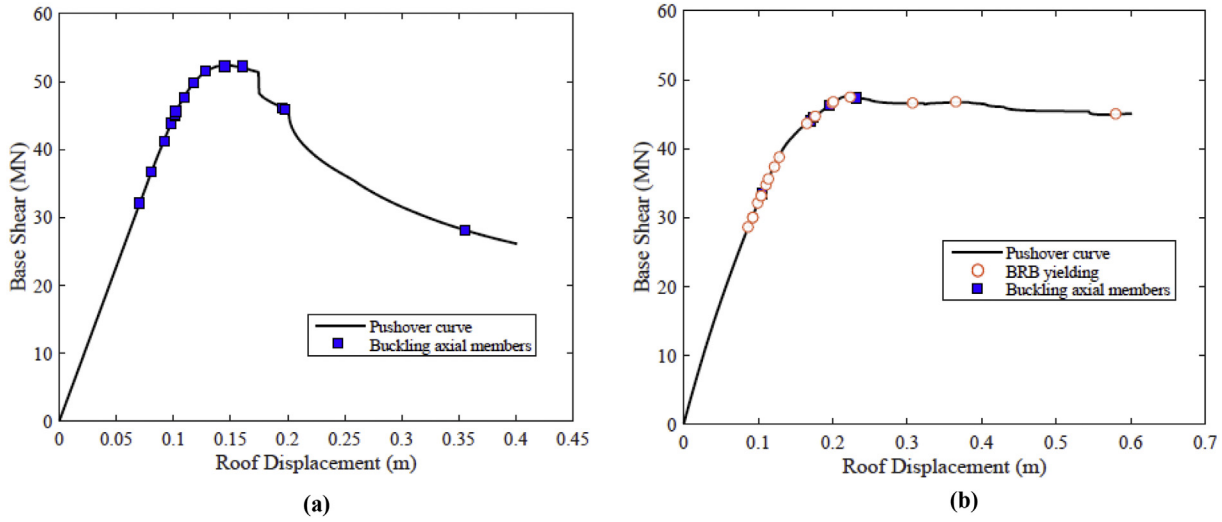

Fig. 12. (a) The buckling sequence of the diagonal members in the initial 8-story-45^0 model, (b) The yielding BRBs of the BRB equipped 8-story-45^0 model.

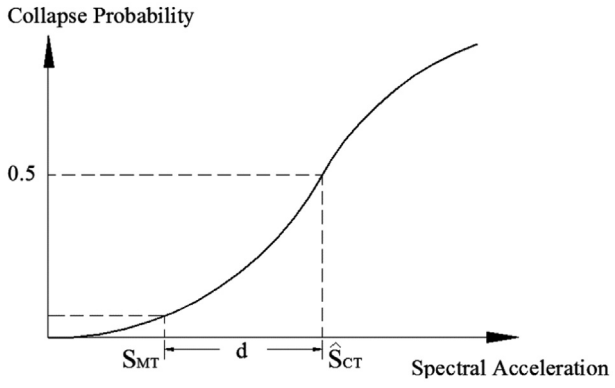

Fig. 13. The collapse probability curve for a particular structure.

motions to be scaled (upward or downward) to reach the point of median collapse capacity. Therefore, as the CMR increases, the safety margin against collapse is augmented and the structures can resist more intensive ground motions [14]. Fig. 13 presents a sample collapse probability curve with the related S_{MT} and $\hat{S}_{CT}$. The parameter d, which is the distance between S_{MT} and $\hat{S}_{CT}$, is a representative of CMR. Since the position of $\hat{S}_{CT}$ is fixed to the point corresponding the probability of 50%, increasing the parameter d, for a particular structure, means decreasing the probability of failure under the excitations with S_{MT} intensities.

$$CMR = \hat{S}_{CT}/S_{MT} \tag{6}$$

The S_{MT} that is approximated from the MCE response spectrum, in turn depends on the seismic region and seismic design category (SDC). In this research, the initial diagrid models are designed according to ASCE/SEI 7-10 [26] for highest intensities of SDC D (SDC D_{max}). The 5% damped acceleration spectra of 44 normalized records for SDC D_{max}, and their median and median plus 1 standard deviation are shown in Fig. 14.

To determine the S_{MT}, the fundamental period of the structural models (T) is evaluated according to section 12-8-2-1 of ASCE/SEI 7-10 [26]:

$$T = 1.4 \times 0.0488H^{0.75} \tag{7}$$

where H is the height of the building. To assess the CMR of the models, $\hat{S}_{CT}$ is evaluated for each model by conducting incremental dynamic analyses (IDA). The $\hat{S}_{CT}$ is defined as the spectral acceleration intensity where half of the scaled far field ground accelerations cause collapse. In dynamic analysis of 3-D structural models under bi-directional input, for each pair of earthquake records two analyses will be performed by changing the directions of the input motions. So, a total of 44 dynamics analyses need to be carried out. However, once the 50% of the records (22 records) cause the collapse of the structural model, the $\hat{S}_{CT}$ can be evaluated without continuing the analyses [14].

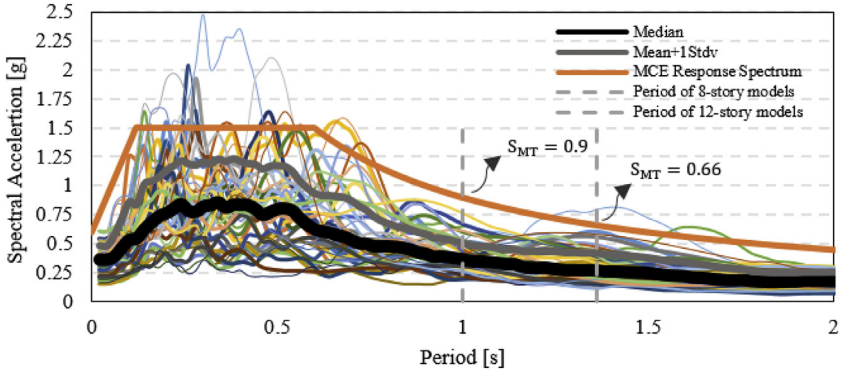

Fig. 14. The 5% damped spectral response accelerations of normalized records, and MCE response spectrum.

Table 6
The results of evaluating CMR for diagrid models.

Model	T	S_{MT}	$\hat{S}_{CT}$	CMR
8-St 45°	1.0	0.9	0.75	0.83
8-St 45° (BRB equipped)	1.0	0.9	1.33	1.48
8-St 63.4°	1.0	0.9	0.67	0.74
8-St 63.4° (BRB equipped)	1.0	0.9	1.4	1.55
8-St 71.5°	1.0	0.9	0.86	0.95
8-St 71.5° (BRB equipped)	1.0	0.9	1.05	1.16
12-St 45°	1.36	0.66	0.56	0.85
12-St 45° (BRB equipped)	1.36	0.66	0.97	1.47
12-St 63.4°	1.36	0.66	0.66	1.0
12-St 63.4°(BRB equipped)	1.36	0.66	0.93	1.41
12-St 71.5°	1.36	0.66	0.66	1.0
12-St 71.5° (BRB equipped)	1.36	0.66	0.88	1.33

As the first step in conducting IDA, each one of a pair of records is normalized relative to the geometric mean of peak ground velocities (PGV_{peer}) of that pair in order to remove the unwarranted variability between records due to inherent differences in event magnitude, distance to source, source type and site conditions, without eliminating record-to-record variability [14]. Next, the normalized pairs of records are scaled upward incrementally and the time history analyses are carried out using the scaled records. For the IDA the damage measure (DM) is considered to be the maximum story drift, while the "median spectral intensity (S_T)" of the scaled records is selected as the intensity measure (IM). Therefore, this approach is somewhat different in comparison to the IDA proposed by Vamvatsikos and Cornell [37].

In case of braced frames subjected to horizontal ground motions, sidesway collapse is a governing mechanism that leads to lateral dynamic instability and collapse of the system. The sidesway collapse occurs when the displacements of any specific story becomes large enough to offset the shear resistance of the structural model, thus causing reduction in their gravity load carrying capacity [38]. Numerical instability due to non-convergence of the time-integration process features sidesway collapse of nonlinear diagrid models in the OpenSees program. Also, the collapse point is observable in IDA curves, when a minor increase in IM causes large increment in DM.

The collapse point is considered as the occurrence of simulated or non-simulated collapse modes. Simulated collapse modes have already been defined and modeled through the nonlinear performance of axial members in the Section 2. But non-simulated collapse modes of diagrid systems are not well known, as the experiments and studies rarely address the seismic behavior of diagrids. Some experiments [18,39,40] indicate that the non-simulated collapse modes of diagrid structures are mainly concentrated in the connection zone. Also, the non-simulated collapse modes of braced and moment frames take place when the drift ratio of the structural models are between 5 and 10%. In the case of diagrid structures, drift ratios generally rise as the diagonal angles increase; as a result, it is expected that the limit states to control the non-simulated collapse modes should be increased by rising the diagonal angles. In this study, the limit states to check the occurrence of non-simulated collapse modes for 45°, 63.4°, and 71.5° models are considered to be 5%, 7%, and 9%, respectively, as suggested by [41].

Results of evaluating CMR are provided in Table 6. Values of S_{MT} are constant for models with equal heights, as S_{MT} is a function of T which is in turn a function of the height of the building models. To investigate the effects of BRBs on the collapse performance of the models, Fig. 15 shows the variations of CMR as a function of diagonal angles. This figure indicates that for the initial diagrids, the values of CMR generally increase by rising the diagonal angles. This trend is reverse in BRB equipped models where the collapse capacity improvement mostly occurs for diagrids with smaller diagonal angles. Fig. 16 shows the IDA curves for the regular and BRB equipped 12-story-71.5° diagrid. The difference between the curves is just due to the record-to-record variability of ground motions. For the initial model, there is no safety margin against

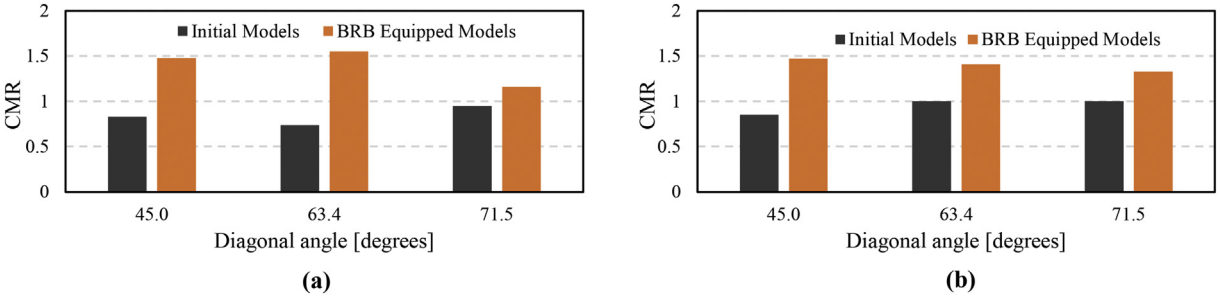

Fig. 15. Variation of CMR vs diagonal angles: (a) 8-story models, (b) 12-story models.

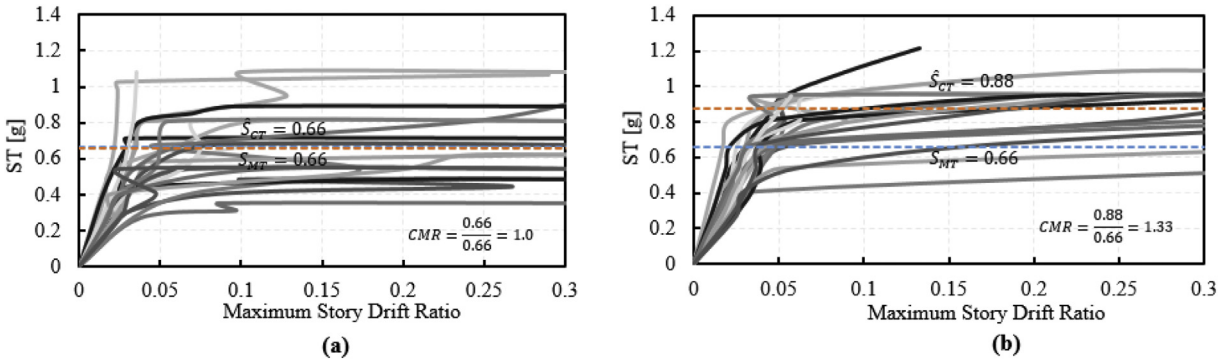

Fig. 16. IDA curves for diagrid models: (a) Initial 12-story-71.5°, (b) BRB equipped 12-story-71.5°.

collapse since $\hat{S}_{CT}$ is equal to S_{MT} and CMR is unity. Equipping this model with BRBs shifts the $\hat{S}_{CT}$ up to 0.88 and improves the collapse capacity by around 33%.

The IDA results are presented in Fig. 17. This figure shows the cumulative distributions of the collapse intensities obtained from IDA results for the initial and the BRB equipped models. The collapse intensity is defined as the maximum drift ratio of the structural model or the spectral acceleration of the records at the onset of collapse. To consider the characteristics of a pair of horizontal records in collapse performance assessment process, the spectral acceleration of a pair of records is described as the geometric mean of 5%-damped spectral acceleration (S_a(T,5%)) of the pair of the bi-directional records:

$$S_a(T,5\%) = \sqrt{S_{a1}(T,5\%) \times S_{a2}(T,5\%)} \tag{8}$$

where S_{ai}(T,5%) is the spectral 5%-damped acceleration of the i_{th} ($i = 1, 2$) record at the fundamental period of the structure. A quick look at the cumulative distribution curves represented in Fig. 17 indicates that equipping diagrid models by BRBs generally shifts the cumulative curves of the initial (without BRB) models to the right. This means that collapse capacity of BRB equipped models is greater than that of the regular models. To better study the effects of adding BRBs on seismic performance of models, the PI is redefined here as the ratio of median damage measure (DM) or intensity measure (IM) of a BRB equipped model to the median DM (or IM) of the initial diagrid:

$$PI = \frac{Median(Drift\ Ratio\ or\ S_a(T,5\%)\ of\ BRB\ equipped\ models)}{Median(Drift\ Ratio\ or\ S_a(T,5\%)\ of\ initial\ models)} \tag{9}$$

Fig. 18 shows the PIs as a function of the diagonal angles. This figure indicates that the PI of collapse drift ratios increases as the diagonal angles increase, so equipping the diagrids by BRB substantially increases the collapse displacements of the diagrids with larger diagonal angles (71.5°). Also, all PIs of the collapse intensities are larger than unity which means that the BRB equipped models can withstand more intense earthquakes. Variation of PI associated with the collapse spectral accelerations has a reverse trend relative to the trend of PI of collapse drifts. In other words, PI of collapse spectral accelerations is larger for diagrids with smaller diagonal angles. This is attributed to the behavior change of the diagrids from braced frames to moment resisting frames as their diagonal angle increases.

6. Conclusion

In this study a new approach for improving the seismic performance of diagrid structures through application of BRBs is proposed. 6 three

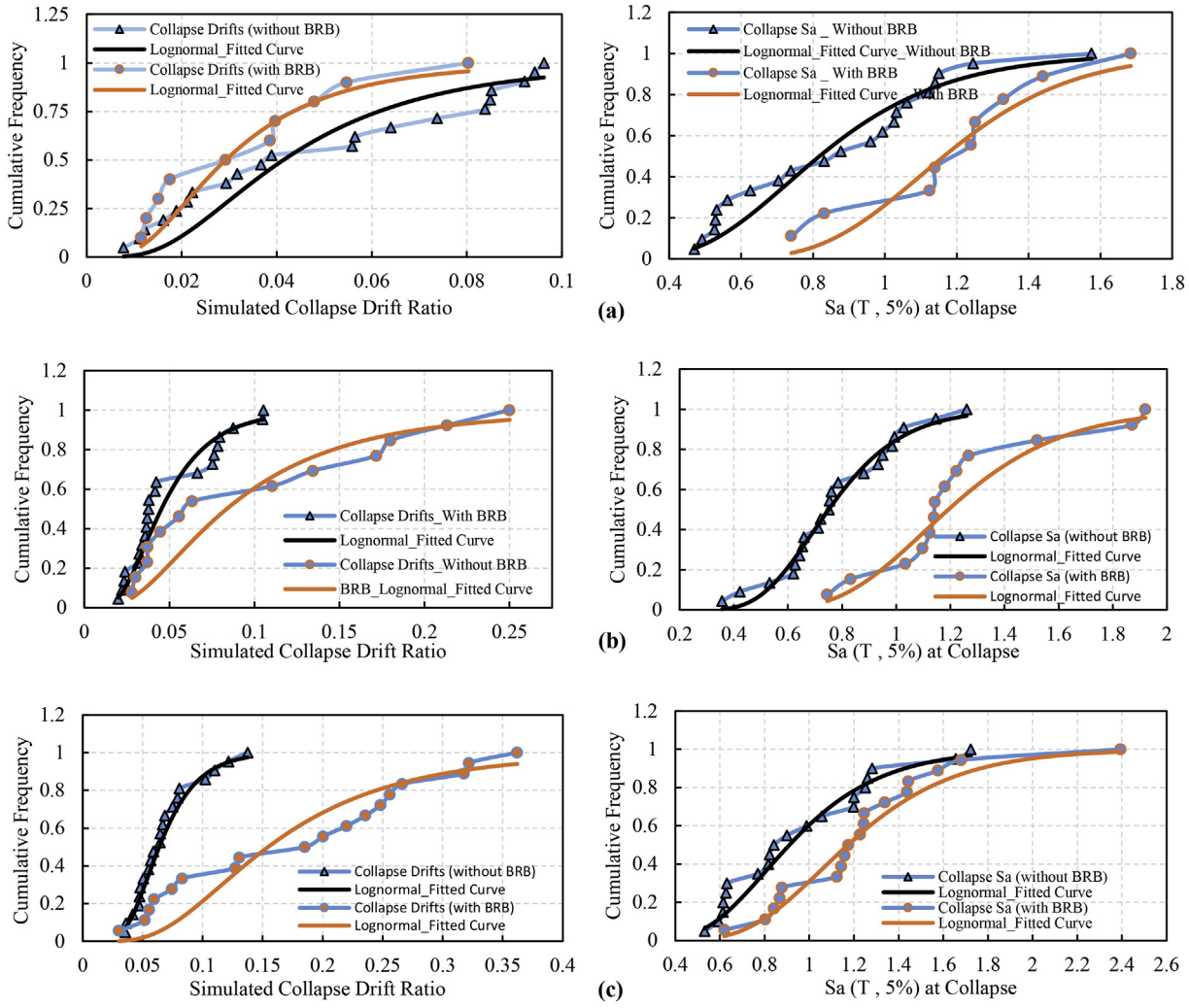

Fig. 17. Cumulative distribution functions for collapse points (left curves: collapse drift ratio, right curves: collapse Sa (T, 5%)): (a) 8-story-45°, (b) 12-story-45°, (c) 8-story-63.4°, (d) 12-story-63.4°, (e) 8-story-71.5°, (f) 12-story-71.5°.

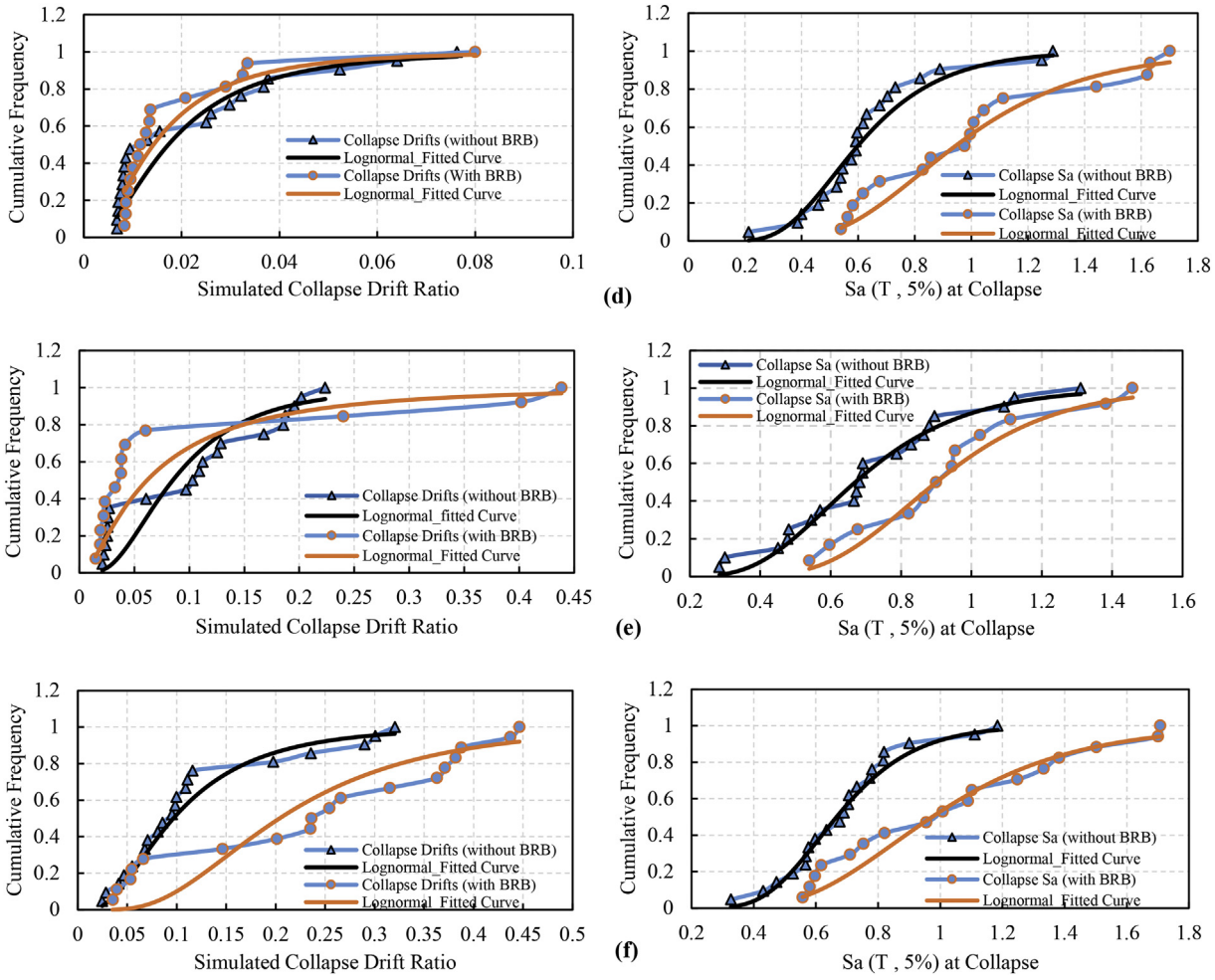

Fig. 17 (*continued*).

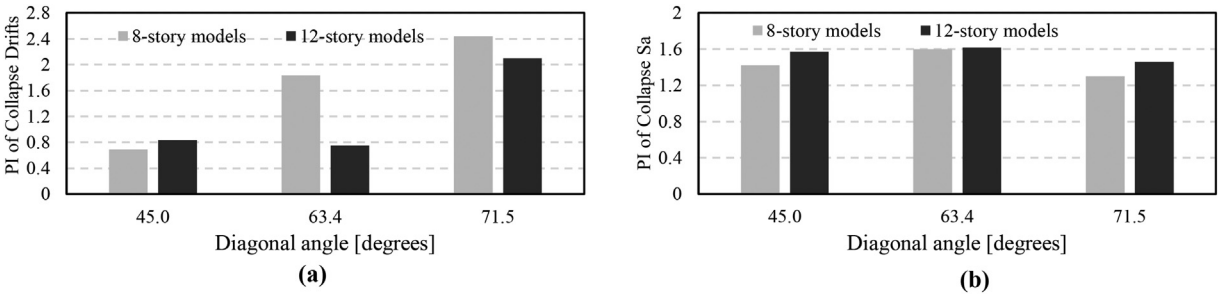

Fig. 18. Variations of PI vs diagonal angles: (a) PI for collapse drifts, (b) PI for collapse Sa (T, 5%).

dimensional nonlinear diagrid models were partially equipped by the BRBs in a suggested arrangement, and nonlinear pushover and time history analyses were conducted. Overally, the obtained results indicated that partially replacement of the diagonal elements by BRBs, as suggested, could improve the seismic performance factors of diagrids by efficiently accumulating the plastic damages in BRBs, thus preventing the remaining diagonals from buckling. Also, the distribution of the plastic behavior of the diagonals becomes more uniform throughout the structure when partially equipped with BRBs. The detailed findings of this study are as the following:

Results of the pushover analyses:

- The over-strength factor (Ω_0) remains almost constant for diagrid models with average value of 1.2 for all models.
- The ductility ratio, μ, of all initial and BRB equipped models generally has an increasing trend with growing diagonal angles. Also, the ductility of 8-story-71.5° models is greater than other cases. It is equal to 2.5 for initial model and 3.1 for BRB equipped model. This can be attributed to the flexural behavior of the diagrids with higher diagonal angles.
- For most cases, both R_μ and R have an increasing trend with rising diagonal angles from 45^0 to 63.4^0. For 12-story models, the diagonal angle of 63.4° seems to be optimal for both R_μ and R not only in the initial models but also in the BRB equipped models. The maximum value of R for the initial models is 2.47 for 8-story-71.5° model, while for the BRB equipped cases is 3.28 for 12-story-63.4° model.
- Generally, PI is greater than one for all models, which demonstrates the improvement in the seismic performance of the models; for

12-story-63.4° model, application of BRB increases the R factor from 1.97 to 3.28, indicating an improvement of 66%.
- In 8-story models, PI of the R factor reduces by growing diagonal angles; so, 8-story-45° model achieves the maximum improvement of 37%.

Results of dynamic analyses:

- The values of CMR for regular models generally increase by growing diagonal angles. But for the BRB-equipped cases, this trend is somehow reverse, indicating that the BRB-equipped models with smaller diagonal angles have a greater safety margin against collapse.
- The cumulative distribution functions of collapse spectral accelerations of BRB-equipped models are located at the right side of cumulative curves for the regular models, showing improvement in the collapse capacity of BRB-equipped diagrids for all statistical levels.
- The maximum value of PI for collapse intensities belongs to the diagrids with diagonal angle of 63.4°. For both 8- and 12-story models with diagonal angle of 63.4°, the collapse intensities are in average improved by up to 60%. For diagonal angles steeper than 63.4°, the effectiveness of using BRB is reduced.
- Diagrids with larger diagonal angles gain more increase in collapse drifts by being equipped with BRBs.

Authors contribution statement

Mr. Saman Sadeghi is one of my graduate students whom obtained his MSc degree in Earthquake Engineering of Civil Engineering Department, Sharif University of Technology, in January 2019. He worked in the area of dynamic characteristics of diagrid structures under my supervision from 2017 to 2019. He has been working on numerical modeling of the diagrid structures using OpenSees program under my Supervision. Also, we did not have any funding for his MSc thesis project.

Declaration of Competing Interest

The authors declare that they have no known competing financial interests or personal relationships that could have appeared to influence the work reported in this paper.

References

[1] G.M. Montuori, E. Mele, G. Brandonisio, A. De Luca, Geometrical patterns for diagrid buildings: exploring alternative design strategies from the structural point of view, Eng. Struct. 71 (2014) 112–127.
[2] M. Goldsmith, The Tall Building: The Effects of Scale, Illinois Institute of Technology, Chicago, 1953.
[3] A. Aminmansour, K.S. Moon, Integrated design and construction of tall buildings, J. Archit. Eng. 16 (June) (2010) 47–53.
[4] T.M. Boake, Diagrid Structures, Systems, Connections, Details, worldsteel Association, Basel, 2014.
[5] G.M. Montuori, E. Mele, G. Brandonisio, A. De Luca, Design criteria for diagrid tall buildings: stiffness versus strength, Struct. Des. Tall Spec. Build. 24 (July 2014) (2014) 421–439.
[6] G.M. Montuori, E. Mele, G. Brandonisio, A. De Luca, Secondary bracing systems for diagrid structures in tall buildings, Eng. Struct. 75 (2014) 477–488.
[7] J. Leonard, J.J. Connor, Investigation of Shear Lag Effect in High-rise Buildings with Diagrid System, Massachusetts Institute of Technology, 2007.
[8] R.J. Liptack, Motion Based Seismic Design and Loss Estimation of Diagrid Structures, 2013.
[9] B.A. Rahimian, Y. Eilon, New York's Hearst tower, Struct. Mag. (February) (2006) 25–29.
[10] C. Besjak, B. Kim, P. Biswas, 555m tall Lotte super tower, Seoul, Korea, Struct. Congr. 2009 (4) (2009) 1–10.
[11] K.S. Moon, J.J. Connor, J.E. Fernandez, Diagrid structural systems for tall buildings: characteristics and methodology for preliminary design, Struct. Des. Tall Spec. Build. 16 (2) (2007) 205–230.
[12] K.S. Moon, Sustainable structural engineering strategies for tall, buildings 17 (5) (2008).
[13] W. Baker, C. Besjak, M. Sakisian, P. Lee, C.S. Doo, Proposed Methodology to Determine Seismic Performance Factors for Steel Diagrid Framed Systems, Counc. Tall Build, Urban Habitat, 2010.
[14] FEMA P695, Quantification of Building Seismic Performance Factors, no. June, Federal Emergency Management Agency, Washington, D.C, 2009.
[15] J. Kim, Y.-H. Lee, Seismic performance evaluation of diagrid system buildings, Struct. Des. Tall Spec. Build. 21 (12) (2012) 867–878.
[16] N.S. Moghaddasi B, Y. Zhang, Seismic analysis of diagrid structural frames with shear-link fuse devices, Earthq. Eng. Eng. Vib. 12 (3) (2013) 463–472.
[17] D. Lee, S. Shin, Advanced high strength steel tube diagrid using TRIZ and nonlinear pushover analysis, J. Constr. Steel Res. 96 (2014) 151–158.
[18] Y.J. Kim, M.H. Kim, I.Y. Jung, Y.K. Ju, S.D. Kim, Experimental investigation of the cyclic behavior of nodes in diagrid structures, Eng. Struct. 33 (7) (2011) 2134–2144.
[19] X. Han, C. Huang, J. Ji, J. Wu, Experimental and numerical investigation of the axial behavior of connection in CFST Diagrid structures, Tsinghua Sci. Technol. 13 (Suppl. 1) (2008) 108–113.
[20] J. Teng, W.L. Guo, B.S. Rong, Z.H. Li, Z.J. Dong, Research on seismic performance objectives of high-rise Diagrid tube structures, Adv. Mater. Res. 163–167 (2011) 1100–1106.
[21] D.K. Lee, U. Starossek, S.M. Shin, Optimized topology extraction of steel-framed DiaGrid structure for tall buildings, Int. J. Steel Struct. 10 (2) (2010) 157–164.
[22] N. Mashhadiali, A. Kheyroddin, Progressive collapse assessment of new hexagrid structural system for tall buildings, Struct. Des. Tall Spec. Build. 23 (12) (2014) 947–961.
[23] L.J. Jia, R.W. Li, P. Xiang, D.Y. Zhou, Y. Dong, Resilient steel frames installed with self-centering dual-steel buckling-restrained brace, J. Constr. Steel Res. 149 (2018) 95–104.
[24] L.J. Jia, H. Ge, P. Xiang, Y. Liu, Seismic performance of fish-bone shaped buckling-restrained braces with controlled damage process, Eng. Struct. 169 (May) (2018) 141–153.
[25] S. Mazzoni, F. McKenna, M.H. Scott, G.L. Fenves, Open System for Earthquake Engineering Simulation (OpenSees), California, Berkeley, 2006.
[26] ASCE 7–10, Minimum Design Loads for Buildings and Other Structures, American Society of Civil Engineers, Reston, Virginia, 2010.
[27] P. Uriz, Towards Earthquake Resistant Design of Concentrically Braced Steel Structures, University of California, Berkeley, 2005.
[28] M. D'Aniello, G.L.M. Ambrosino, F. Portioli, R. Landolfo, The influence of out-of-straightness imperfection in physical theory models of bracing members on seismic performance assessment of concentric braced structures, Struct. Des. Tall Spec. Build. 24 (2015) 176–197.
[29] J. Bai, J. Ou, Earthquake-resistant design of buckling-restrained braced RC moment frames using performance-based plastic design method, Eng. Struct. 107 (2016) 66–79.
[30] S. Merrit, C. Uang, G. Benzoni, Subassemblage Testing of Corebrace Bucklingrestrained Braces, San Diego, La Jolla, CA 2003.
[31] A. Zona, A. Dall'Asta, Elastoplastic model for steel buckling-restrained braces, J. Constr. Steel Res. 68 (1) (2012) 118–125.
[32] M. Iwata, T. Kato, A. Wada, Buckling-restrained braces as hysteretic dampers, in: F.M. Mazzolani, R. Tremblay (Eds.), Behav. Steel Struct. Seism. Areas, STESSA, Balkema 2000, pp. 33–38.
[33] C. Chou, S. Chen, Subassemblage tests and finite element analyses of sandwiched buckling-restrained braces, Eng. Struct. 32 (8) (2010) 21no. 2108.
[34] P.W. Clark, I.D. Aiken, F.F. Tajirian, K. Kasai, K. Ko, I. Kimura, Design procedures for buildings incorporating hysteretic damping devices, International Post-SmiRT Conference Seminar on Seismic Isolation, Passive Energy Dissipation andActive Control of Vibrations of Structures, 1999.
[35] ASCE 41–13, Seismic Evaluation and Retrofit of Existing Buildings, Reston, Virginia, Federal Emergency Management Agency, 2014.
[36] C. Uang, Establishing R (or Rw) and Cd Factors for Building Seismic Provisions, J. Struct. Eng. 117 (1) (1991) 19–28ASCE 19-28.
[37] D. Vamvatsikos, C.A. Cornell, The incremental dynamic analysis and its application to performance-based earthquake engineering, Eur. Conf. Earthq. Eng. (2002) 10.
[38] E. Karamanci, D.G. Lignos, Computational approach for collapse assessment of concentrically braced frames in seismic regions, J. Struct. Eng. 140 (8) (2014) A4014019.
[39] B.V. Fell, A.M. Kanvinde, G.G. Dierlein, Large Scale Testing and Simulation of Earthquake Induced Low Cycle Fatigue in Bracing Members Subjected to Cyclic Inelastic Buckling, 2010.
[40] D. Lehman, C. Roeder, Improved seismic design of concentrically braced frames and gusset plate connections, Struct. Congr. (2008) 1–10, 2008.
[41] S. Sadeghi, F.R. Rofooei, Quantification of the seismic performance factors for steel diagrid structures, J. Constr. Steel Res. 146 (2018) 155–168.